

Supporting Informations

Uniform Lithium ion flux and robust interphase enabled by anion anchoring additive for high energy density Si-based anodes

Jinhyung Kim^{a,†}, SeungEun Yu^{a,†}, Haein Park^a, Jaehoon Yoon^a, Chanho Lee^a, Ryeowon Kang^a, Kyobin Park^a, San Moon^b, Patrick Joohyun Kim^c, Seho Sun^d, Ki-Min Roh^e, Incheol Jeong^{e,}, Dongsoo Lee^{a,*} and Junghyun Choi^{a,*}*

^aSchool of Chemical, Biological and Battery Engineering, Gachon University, 1342 Seongnam-daero, Sujeong-gu, Seongnam 13120, Republic of Korea. E-mail: dslee9117@gachon.ac.kr, junghchoi@gachon.ac.kr

^bAdvanced Battery Research Center, Korea Research Institute of Chemical Technology, Daejeon, 34114, Republic of Korea

^cSchool of Chemical Engineering and Applied Chemistry, Kyungpook National University, Daegu, 41566, Republic of Korea

^dSchool of Chemical Engineering, Yeungnam University, Gyeongsan, 38541, Republic of Korea

^eResources Utilization Research Center, KIGAM, Daejeon 34132, Republic of Korea, E-mail: icjeong@kigam.re.kr

† These authors contributed equally to this work

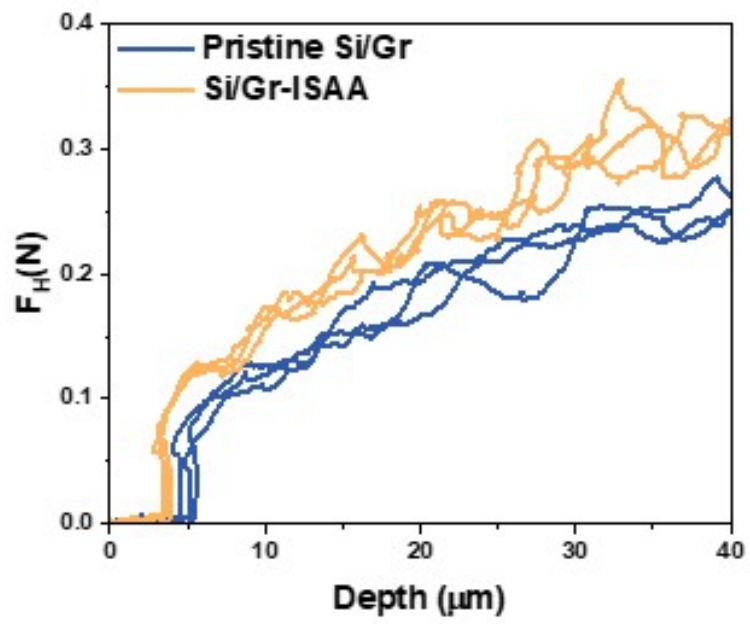


Fig. S1 Depth-dependent shear force profiles of pristine Si/Gr and Si/Gr-ISAA electrodes measured by SAICAS.

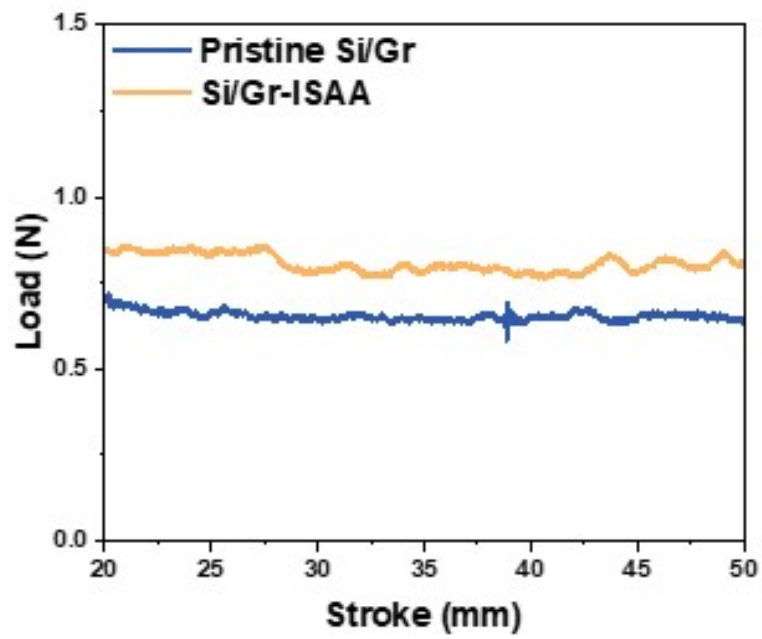


Fig. S2 Load-stroke profiles of pristine Si/Gr and Si/Gr-ISAA electrodes measured by UTM peel testing.

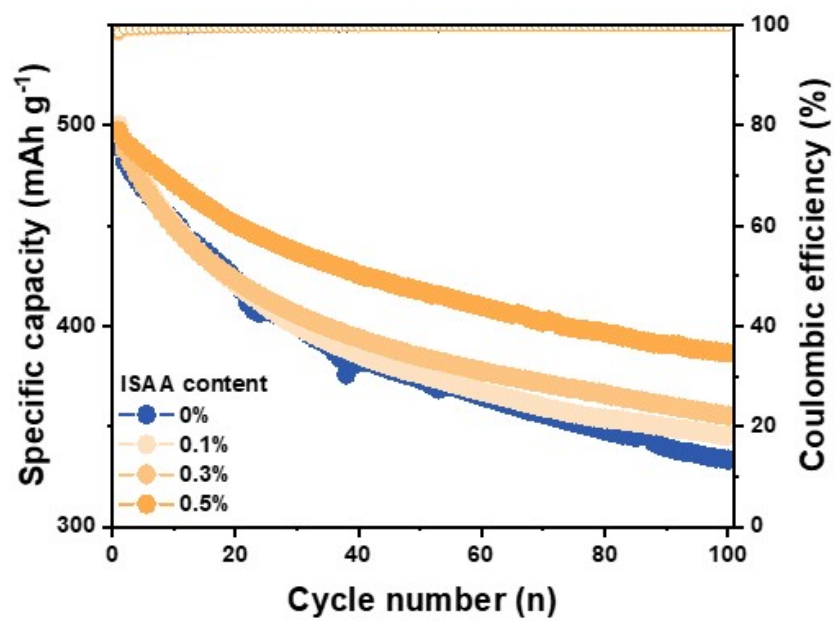


Fig. S3 Cycling performance of Si/Gr composite anodes with different ISAA contents.

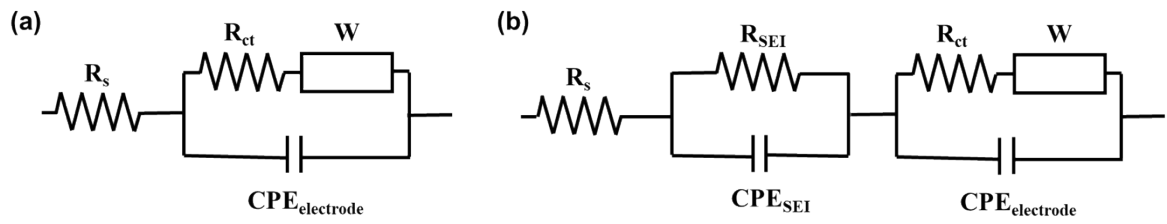


Fig. S4 Equivalent circuits for the Nyquist plots. (a) Randles circuit and (b) dual-interface model including R_{SEI} and CPE_{SEI} for SEI layer characterization. R_s , R_{ct} and W denote ohmic resistance, charge transfer resistance, and Warburg impedance, respectively.

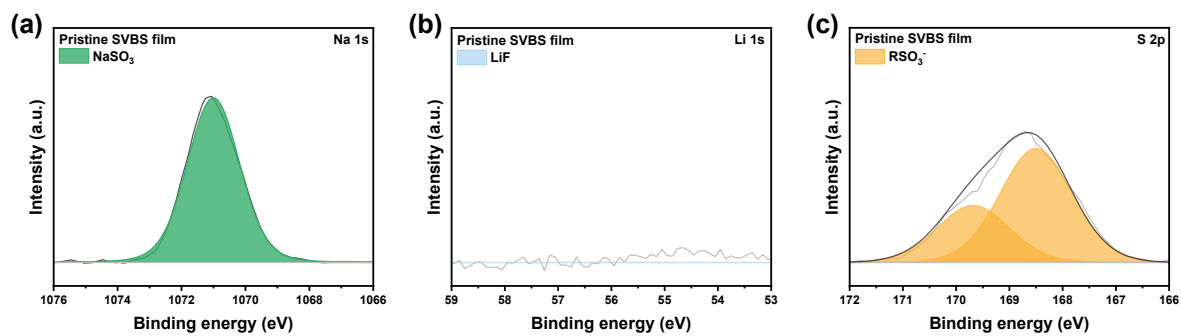


Fig. S5 XPS analysis of the pristine SVBS film. (a) Na 1s spectrum. (b) Li 1s spectrum. (c) S 2p spectrum.

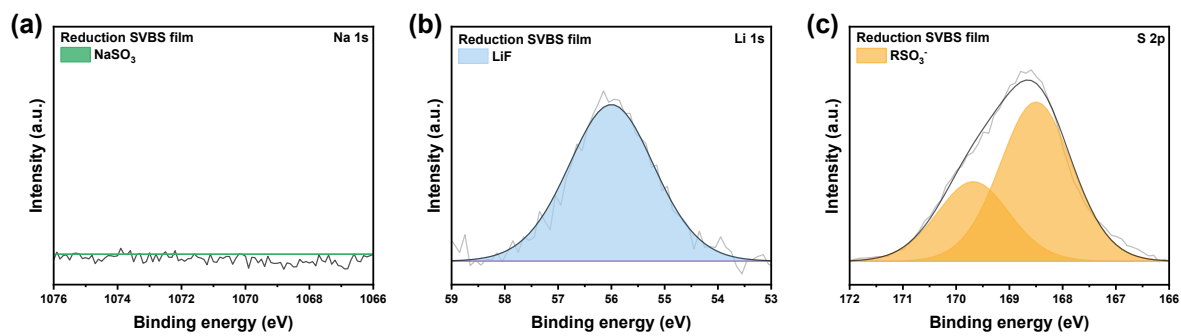


Fig. S6 XPS analysis of the pristine SVBS film. (a) Na 1s spectrum. (b) Li 1s spectrum. (c) S 2p spectrum.



Fig. S7 Non-uniform lithium deposition observed on the pristine Si/Gr electrode after 30 cycles.

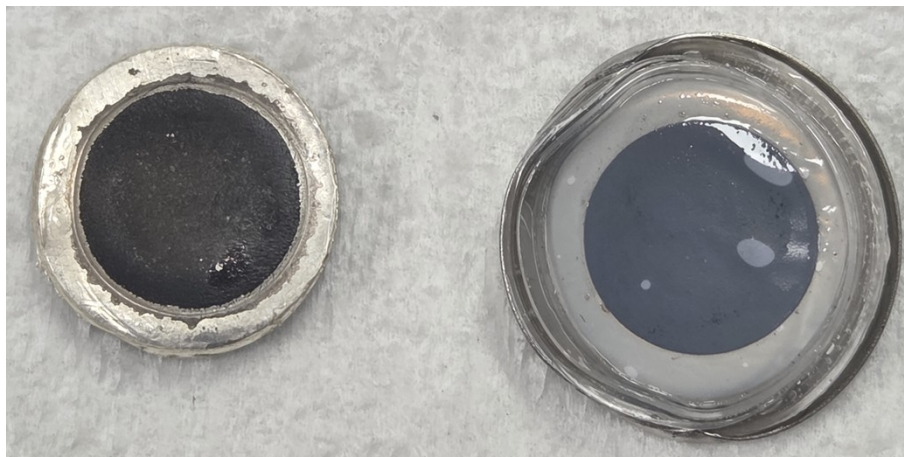


Fig. S8 Uniform lithium deposition observed on the Si/Gr-ISAA electrode after 30 cycles.

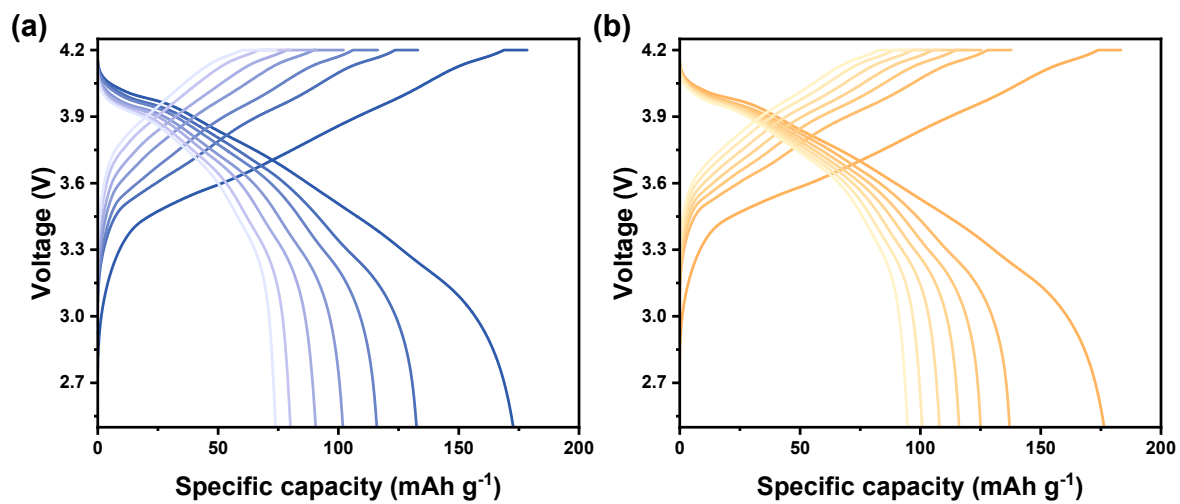


Fig. S9 Full-cell cycle performance of (a) pristine Si/Gr and (b) Si/Gr-ISAA electrodes at a C-rate of 0.5C.

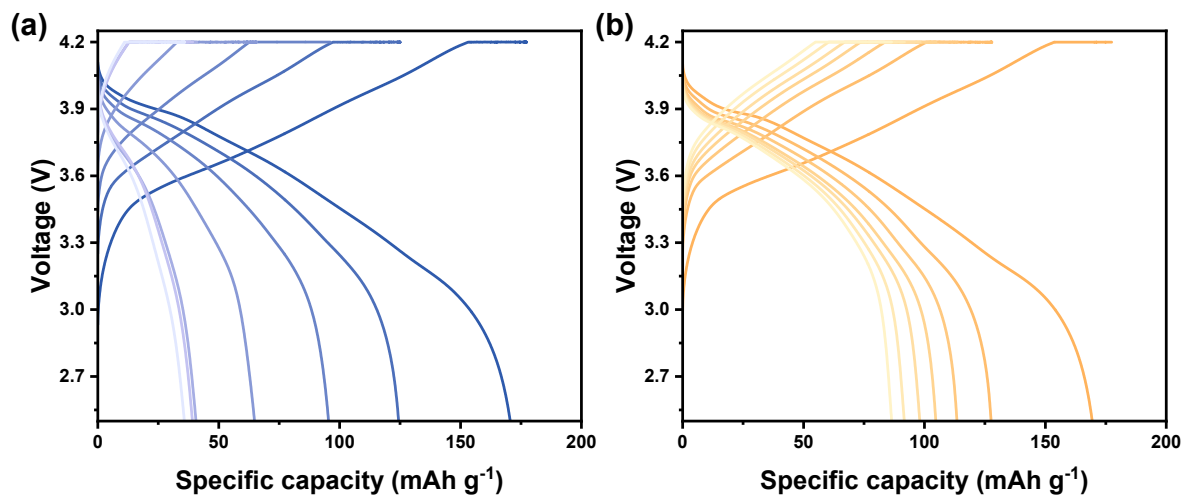


Fig. S10 Full-cell cycle performance of (a) pristine Si/Gr and (b) Si/Gr-ISAA electrodes at a C-rate of 1C.

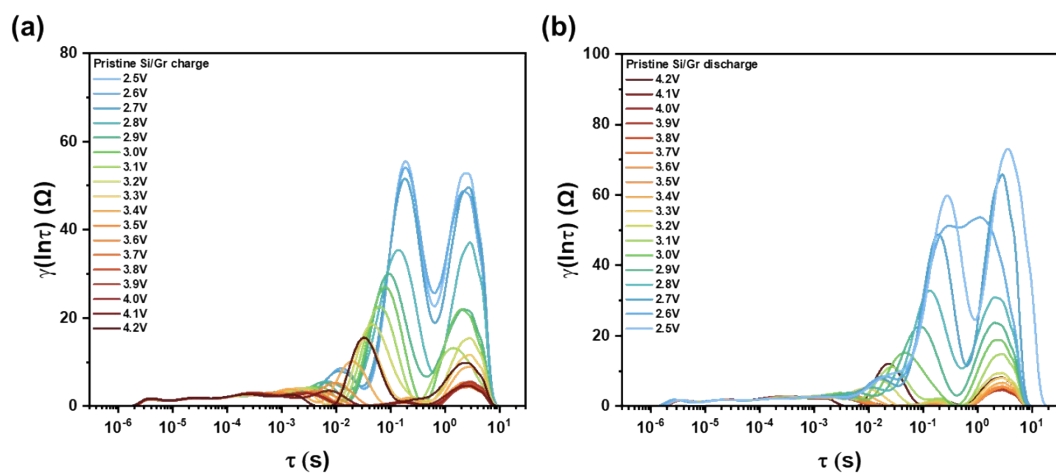


Fig. S11 DRT analysis of pristine Si/Gr electrode (a) charge (b) discharge cycle.

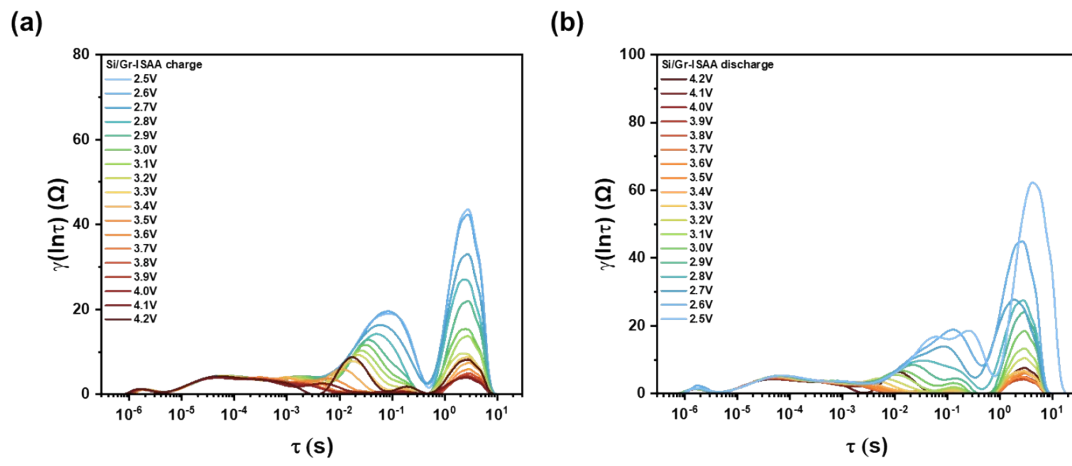


Fig. S12 DRT analysis of Si/Gr-ISAA electrode (a) charge (b) discharge cycle.

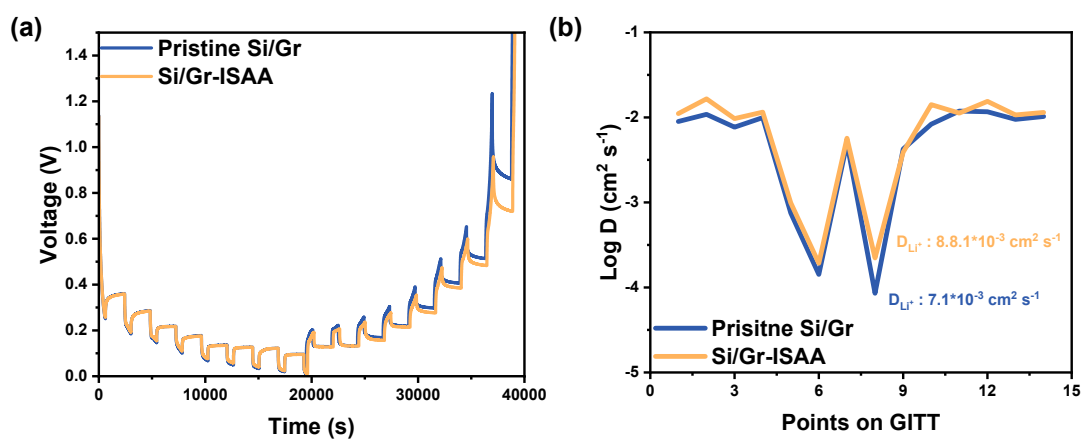


Fig. S13 GITT analysis of (a) pristine Si/Gr and (b) Si/Gr-ISAA electrodes.

Table S1. Summary of electrode design parameters for the Si/Gr composite anode and corresponding full-cell configuration, including areal capacity, N/P ratio and electrolyte amount.

Parameter	Unit	Cathode	Anode
Active material loading	mg cm ⁻²	15.9	6.6
Electrode density	g cm ⁻³	3.0	1.5
Specific capacity	mAh g ⁻¹	200	530
Areal capacity	mAh cm ⁻²	3.18	3.5
Full-Cell			
N/P ratio	-		1.1
Electrolyte amount	μL		50
E/C ratio	μL mAh ⁻¹		20

Governing Equations

The electrolyte-phase mass conservation in the P2D framework is governed by:

$$\partial C_e / \partial t = \nabla(D_{e,eff} \nabla C_e) + (1 - t_{Li^+}^t) a_s j_{BV} / F \quad (1)$$

where C_e is the electrolyte Li^+ concentration, $D_{e,eff}$ is the effective electrolyte diffusion coefficient, $t_{Li^+}^t$ is the cation transference number, a_s is the specific interfacial area, j_{BV} is the Butler–Volmer reaction current density, and F is the Faraday constant. The source term is directly proportional to the factor ($t_{Li^+}^t$), which represents the fraction of ionic current carried by the anion. Thus, increasing $t_{Li^+}^t$ directly reduces the rate of electrolyte concentration depletion during galvanostatic operation.

At steady state ($\partial C_e / \partial t = 0$), the local concentration gradient scales linearly with the applied current density and inversely with $D_{e,eff}$. The concentration depletion $\Delta C_e = C_{e,0} - C_{e,min}$ at the current collector is proportional to $(1 - t_{Li^+}^t)$, yielding a theoretical depletion ratio between two systems with different $t_{Li^+}^t$:

$$\Delta C_{e,Pristine} / \Delta C_{e,ISAA} = (1 - t_{Li^+,Pristine}^t) / (1 - t_{Li^+,ISAA}^t) = 0.80 / 0.41 = 1.951 \quad (2)$$

Model parameters

Two electrode configurations were compared: a pristine electrode and an ISAA-modified electrode. The key distinction is the enhanced cation transference number ($t_{Li^+}^t = 0.59$) achieved by the ISAA additive, compared to the conventional liquid electrolyte value ($t_{Li^+}^t = 0.20$). This increase is attributed to the selective immobilization of anions by the ISAA framework, which restricts PF_6^- mobility while maintaining Li^+ transport pathways^{1,2}. Additionally, the ISAA electrode exhibits a lower charge transfer resistance ($R_{ct} = 80 \Omega \cdot cm^2$ vs. $181.5 \Omega \cdot cm^2$), corresponding to a higher exchange current density ($i_0 = 0.183 \text{ A m}^{-2}$ vs. 0.081 A m^{-2}). The remaining model parameters are summarized in Table S2 of the main text.

Parameter	Symbol	Value	Unit
Initial electrolyte conc.	$C_{e,0}$	1150	Mol m^{-3}
Electrode thickness	L_{neg}	47	μm
Separator thickness	L_{sep}	20	μm
Effective diffusivity	$D_{e,eff}$	4.27×10^{-11}	$\text{m}^2 \text{ s}^{-1}$
Ionic conductivity	$K_{e,eff}$	0.140	S m^{-1}
1C current density	I_{1C}	35	A m^{-2}
Transference no. (Pristine)	$t_{Li^+}^t$	0.20	-
Transference no. (ISAA)	$t_{Li^+}^t$	0.59	-

Table S2. P2D Model Parameters

References

- 1 K. Xu, *Chem. Rev.*, 2004, **104**, 4303–4418.
- 2 R. Bouchet, S. Maria, R. Meziane, A. Aboulaich, L. Lienafa, J. P. Bonnet, T. N. Phan, D. Bertin, D. Gimes, D. Devaux, R. Denoyel and M. Armand, *Nat Mater*, 2013, **12**, 452–457.